Crater formation and deuterium production in laser irradiation of polymers with implanted nano-antennas

László P. Csernai,[1,2,3,4] Igor N. Mishustin,[3] Leonid M. Satarov,[3] Horst Stöcker,[3,5,6] Larissa Bravina,[7] Mária Csete,[8,9] Judit Kámán,[1,8] Archana Kumari,[1,8] Anton Motornenko,[3] István Papp,[1,8] Péter Rácz,[1,8] Daniel D. Strottman,[10] András Szenes,[8,9] Ágnes Szokol,[1,8] Dávid Vass,[7,9] Miklós Veres,[1,8] Tamás S. Biró,[1,11] and Norbert Kroó[1,12]
(NAPLIFE Collaboration)

[1]*Wigner Research Centre for Physics, 1121 Budapest, Hungary*
[2]*Deptartment of Physics and Technology, University of Bergen, 5007 Bergen, Norway*
[3]*Frankfurt Institute for Advanced Studies, 60438 Frankfurt am Main, Germany*
[4]*Csernai Consult Bergen, 5119 Ulset, Norway*
[5]*GSI Helmholtzzentrum für Schwerionenforschung GmbH, 64291 Darmstadt, Germany*
[6]*Institute für Theoretische Physik, Goethe Universität, 60438 Frankfurt am Main, Germany*
[7]*Department of Physics, University of Oslo, N-0316 Oslo, Norway*
[8]*National Research, Development and Innovation Office of Hungary, 1077 Budapest, Hungary*
[9]*Deptartment of Optics and Quantum Electronics, University of Szeged, 6720 Szeged, Hungary*
[10]*Los Alamos National Laboratory, Los Alamos, New Mexico 87545, USA*
[11]*University Babes-Bolyai, 400347 Cluj-Napoca, Romania*
[12]*Hungarian Academy of Sciences, 1051 Budapest, Hungary*

(Received 7 December 2022; accepted 10 July 2023; published 11 August 2023)

Recent validation experiments on laser irradiation of polymer foils with and without implanted golden nanoparticles are discussed. First we analyze characteristics of craters, formed in the target after its interaction with the laser beam. Preliminary experimental results show significant production of deuterons when both the energy of laser pulse and concentration of nanoparticles are high enough. We consider the deuteron production via the nuclear transmutation reactions $p + C \to d + X$ where protons are accelerated by the Coulomb field generated in the target plasma. We argue that maximal proton energy can be above threshold values for these reactions and the deuteron yield may noticeably increase due to presence of nanoparticles.

DOI: 10.1103/PhysRevE.108.025205

I. INTRODUCTION

Relativistic heavy-ion collisions have shown that the hadronization (or burning) of created matter is a very fast, nearly simultaneous process in proper time. This is in contrast to the classical Rayleigh-Hugoniot-Taub detonation theory. The possibility of relativistic detonation on a timelike hyper surface was theoretically discovered in 1987 [1], and was later applied to simulate pellet fusion in Ref. [2]. It was found that it is not possible to obtain a better result than was reached in NIF experiments, where Rayleigh-Taylor instabilities prevented the full burning of the target fuel.

To remedy this problem, we have suggested [3,4] to implant golden nanoparticles (nano-antennas) into the target. In this way one can achieve "timelike" ignition, which occurs nearly simultaneously in the whole target volume. Below we describe the validation experiments within the Nanoplasmonic Laser Induced Fusion Energy (NAPLIFE) project [5]. They are planned in two steps: (i) verification of the amplified absorption of the laser energy in the target with nanoparticles, and (ii) testing a simultaneous detonation in the whole target volume, induced by two short ($\tau \lesssim 1$ fs) laser pulses radiating opposite sides of a flat target.[1]

For the validation tests we have chosen the polymer urethane dimethacrylate (UDMA) (see below), which is hard enough to make thin (3 μm) layers of it and construct an altogether 21 μm multilayer target. By adjusting the nanoparticle (NP) density profile one can achieve [8] simultaneous light absorption in the whole volume.

Recently we started validation experiments where a thicker (∼160 μm) target was irradiated from one side leading to the formation of a crater [9,10].

II. CRATER FORMATION

A. Composition of the target

The urethane dimethacrylate (UDMA) polymer contains 470 nucleons and 254 electrons in 71 atoms. Its molecular formula is $C_{23}H_{38}N_2O_8$. The calculated mass of this molecule equals 470.2628 amu [11].

After the irradiation by an energetic laser pulse the UDMA molecule may fragment and break up to pieces. In this process numerous chemical configurations, e.g., $2(NO_2)$,$2(CO_2)$,CH_4,$C_{16}H_{34}$,4C, or even single atoms may appear in the final state. At large enough laser energies, recombination of nucleons becomes also possible, and new atomic species can be formed. For example, a neutron from ^{13}C may be transferred to a hydrogen, producing a deuterium.

[1]The two-sided irradiation was applied earlier in Refs. [6,7].

This is an endothermic reaction, which requires more energy than needed for the molecular fragmentation.

As far as we know, the deuterium formation in laser irradiated targets was observed in these validation experiments for the first time. It is interesting that its amount strongly increases with raising density of implanted golden nano-antennas [9].

In our validation experiments, we have irradiated three types of thick targets: pure UDMA without nano-antennas (Au0), as well as UDMA with golden nanorod antennas of the size 25×85 nm and volume $V_{\rm Au} \simeq 41724\,{\rm nm}^3$. We have used targets with two different mass density ratios of NPs: $m_{\rm Au}/m_U = 0.126\%$ (Au1) and 0.182% (Au2). It was observed that laser shots break out craters in the UDMA target. Parameters of these craters were analyzed by microscope. It was found that they depend significantly on the concentration of NPs.

B. Craters with nanoplasmonics

Geometrical parameters of craters were measured in Refs. [12–14]. The laser beam with a Gaussian intensity profile was focused to a spot with diameter of 24.5 ± 3.2 μm up to 85% norm (FWHM $\simeq 14.4$ μm, the shape was not circularly symmetric) [15].

The following values of crater diameters have been obtained: 110–130 μm at the laser pulse energy $E_L = 5$ mJ, 120–130 μm at $E_L = 10$ mJ, 130–150 μm at $E_L = 15$ mJ, 155–165 μm at $E_L = 20$ mJ, and 190–200 μm at $E_L = 25$ mJ. The average crater depths, calculated from observed crater volumes and diameters (assuming its cone shape), are as follows: 5.0, 5.2, 5.7 μm at $E_L = 5$ mJ, 7.7, 9.6, 15.6 μm at $E_L = 15$ mJ, and 5.6, 6.7, 14.3 μm at $E_L = 25$ mJ, for the targets Au0, Au1, Au2, respectively. As the effective focus of the laser beam was fixed to about 12.6 μm, the observed increase of the crater diameter could be attributed to the transverse expansion of hot plasma created by the laser beam. One can see that the crater diameters do not depend much on the concentration of nano-antennas. On the other hand, the crater volumes and depths clearly depend on it, see Figs. 1 and 2.

One can see in Fig. 1 that the crater volume V_{cr} increases with the laser pulse energy and with the density of nano-antennas. As compared to the pure UDMA target (Au0), the crater volume increases with E_L more rapidly for targets with nano-antennas (Au1 and Au2). Changing the nanorod antenna density from zero (Au0) to 0.182% (Au2) increases the crater volume from 50 000 to 135 000 μm^3. Thus, the nano-antennas increase the laser light absorption. The largest crater volume $V_{cr} = 135\,000\,\mu{\rm m}^3$ was observed in the experiment Au2 at $E_L = 25$ mJ.

It is interesting to note that the crater volume increases faster than the deposited laser energy. This indicates that the energy of excavating the crater is appreciably larger than the energy directly coming from the laser. An additional energy may come from exothermic chemical reactions during the fragmentation of UDMA, which are neglected in the present analysis.

The average distance between nano-antennas in the unperturbed target can be estimated as

$$\langle L_{\rm AuX}\rangle = [V_{\rm Au}(\rho_{\rm Au}/\rho_U)(m_U/m_{\rm AuX})]^{1/3}, \qquad (1)$$

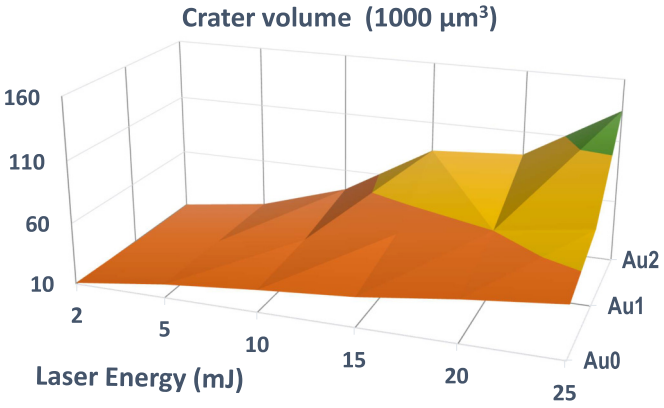

FIG. 1. The crater volume V_{cr} in the thick UDMA target (in units of 1000 μm^3) as the function of laser pulse energy E_L. Several types of targets are considered: Au1 and Au2 with implanted nanorod antennas, and Au0 without implantation. The mass concentrations of implanted particles in UDMA are 0.126% and 0.182% for targets Au1 and Au2, respectively. For each target type five pulse energies are considered. At the highest pulse energy the crater volume increases rapidly with increasing implantation density. For more details, see Refs. [9,12].

where $V_{\rm Au}$ and $\rho_{\rm Au} \simeq 19.32\,{\rm g/cm}^3$ are, respectively, the volume and mass density of a single NP, and $\rho_U \simeq 1.14\,{\rm g/cm}^3$ is the mass density of a pure UDMA material. Using Eq. (1), one gets the values $\langle L_{\rm Au1}\rangle = 0.82$ μm and $\langle L_{\rm Au2}\rangle = 0.73$ μm. This relatively sparse implantation is well visible on the image of the irradiated Au1 and Au2 targets [13]. In the crater image one can clearly see irregular "cracks" associated with nanorod positions [14]. We think that these cracks are formed after "explosion" of nanorods located near the bottom of the crater.

C. Energy densities in target

Let us assume that the laser pulse energy E_L is totally transferred to the internal energy of target matter contained (initially) in the crater volume V_{cr}. Then one can roughly

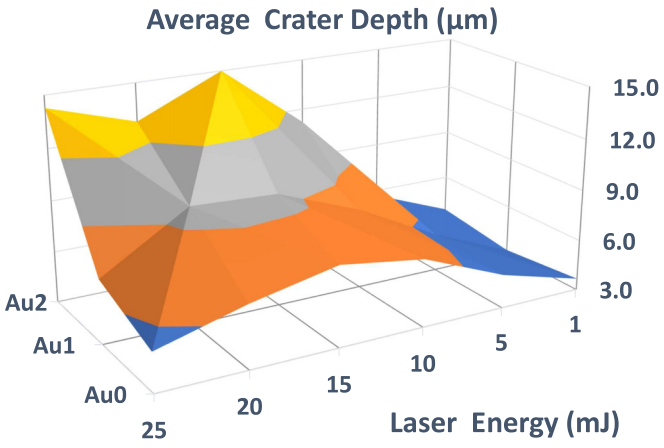

FIG. 2. Average crater depth assuming a circular cone shape as a function of the energy of the laser irradiation E_L and the type of target material. The depth is minimal (3.7–7.7 μm) without nanorod antennas (Au0), while for Au2 target it increases from 5.7 to 15.6 μm.

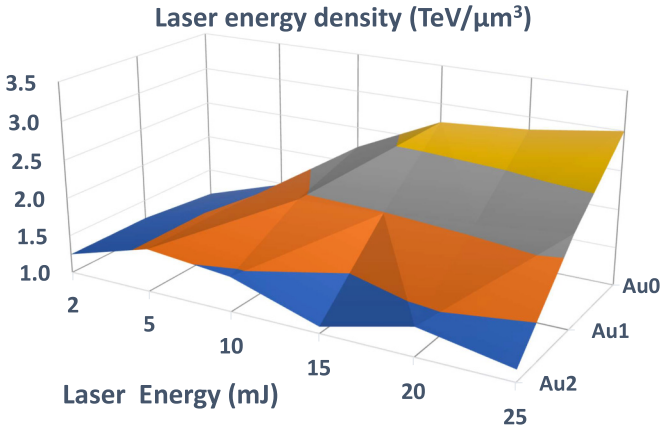

FIG. 3. The laser pulse energy divided by the volume of the crater E_L/V_{cr}. The average energy density in the crater of the target is not directly measurable. In the Au2 target the laser energy is mostly absorbed in the crater, while in two other cases a larger part of the laser energy is passed through or reflected out of it. So more laser irradiation energy is needed to produce the same crater size.

estimate the average energy density deposited in the target as $\varepsilon_{cr} = E_L/V_{cr}$ This gives the results shown in Fig. 3. One can see that $\varepsilon_{cr} \sim 1\,\mathrm{TeV}/\mu\mathrm{m}^3$ for the top laser energy and NP density. The energy density from the laser beam at higher E_L and implantation density decreases, because the crater volume increases more rapidly.[2] This effect indicates that the nanorods cause an additional absorption of laser energy, this is why we call them antennas.

In the case of $E_L = 25$ mJ and the Au2 target one can estimate the energy absorbed by a single NP as $\epsilon_{cr} V_{\mathrm{Au}} \sim 50$ MeV, where V_{Au} is the volume of a single nanorod. In this case the initial number of nano-antennas in the crater volume is about $V_{cr}/\langle L_{\mathrm{Au2}}\rangle^3 \simeq 347000$.

Note, however, that these energy estimates are very crude. In fact, interaction of a short laser pulse with a dense target is a very complicated, space-time dependent process. Presumably, at an early stage the laser beam excites a target in a focal cylindrical channel, which is much more narrow compared to a crater region formed at late times. A part of laser energy goes to ionization of the target's atoms, leading to formation of electron-ion plasma. Under influence of electric fields and microscopic collisions the target particles accelerate and some of them may escape from the crater region. The plasmon excitations in nano-antennas may create "hot spots" in surrounding matter with enhanced energy density [16,17].

III. DEUTERIUM PRODUCTION IN IRRADIATED TARGET

A. Experimental results

As a result of laser irradiation, many electrons as well as molecular and atomic ions are formed in the target. To our surprise, in the experiments with implanted NPs we have observed [9,18] a significant fraction of deuterium atoms, which are emitted on the level of up to 10% of the observed hydrogen numbers D/(2D+H). Here D and H are the *observed* yields of deuterium and hydrogen *atoms*, both determined from the LIBS spectra [10], measured at 0.5 microsecond delay time after the laser pulse [18]. These atoms were detected by presence of Balmer-α lines in the radiation of the H and D, at $\lambda = 656.27$ nm and 656.11 nm, ($E_{B\alpha} = 0.944\,623$ eV and 0.944 843 eV), respectively. The absolute amounts of *observed* H and D were not measured. The relative amount of deuterium atoms increases linearly with the laser beam energy, reaching 7% of hydrogen at $E_L = 25$ mJ with a target including nanorod antennas with mass density of 0.126% (Au1) [19]. One should note that both H and D LIBS spectra exhibit event-by-event fluctuations and these fluctuations are stronger for deuterium.

We have checked that originally the polymer foils used in our experiments did not contain deuterium. Below we analyze possible mechanisms of D production.

B. Nuclear transmutation reactions

Let us first assume that D atoms appear due to electron capture (inverse β decay)

$$p + e \to n + \nu, \tag{2}$$

followed by the $n + p \to d$ fusion [20]. The reaction Eq. (2) is endothermic, and may occur if the kinetic energy of the electron exceeds 783 keV in the laboratory frame. The fusion of n and p is exothermic process:

$$n + p \to d + 2.225\,\mathrm{MeV}. \tag{3}$$

Note that this reaction requires an additional (spectator) particle. However, the reaction Eq. (2) is a weak process with a very small cross section. Therefore, this mechanism cannot explain the observed yield of deuterium [21].

Below we focus on one important aspect of the UDMA fragmentation process, which may lead to nuclear transmutation reactions. Especially interesting are the reactions associated with carbon atoms in the UDMA molecule. Note that a natural carbon is the mixture of two stable isotopes: 98.9% of ^{12}C and 1.06% of ^{13}C. Fast protons accelerated by laser irradiation may lead to production of deuterons via the stripping reactions

$$p + {}^{13}\mathrm{C} \to d + {}^{12}\mathrm{C} \tag{4}$$

and

$$p + {}^{12}\mathrm{C} \to d + {}^{11}\mathrm{C}. \tag{5}$$

These reactions are endothermic and may occur if the proton energy exceeds some minimal (threshold) value. The last neutron in the ground state of the isotope ^{13}C is relatively weakly bound, with the binding energy of about 4.95 MeV. On the other hand, the neutron separation energy of ^{12}C equals approximately 15.65 MeV. Due to this reason, the threshold proton energy required for the reaction Eq. (5) is larger than for the reaction Eq. (4) (see below).

[2]It is clear that the energy of the laser beam should not be equal to the energy absorbed by the target matter, since a part of the beam is reflected.

Let us first consider reaction Eq. (4). It has a negative Q value[3]

$$Q = m(^{13}\mathrm{C}) + m_p - m(^{12}\mathrm{C}) - m_d \simeq -2.7216\,\mathrm{MeV}. \quad (6)$$

Therefore, it can only take place if protons created during the laser-target interaction have sufficiently high kinetic energies (see below).

The inverse "pick-up" reaction

$$d + {}^{12}\mathrm{C} \to p + {}^{13}\mathrm{C} \quad (7)$$

is exothermic. It was extensively studied experimentally in the past (see, e.g., Refs. [23–25]).

The ratio of the cross sections for the pick-up and stripping reactions can be calculated by using the detailed balance relation [26]

$$\frac{\sigma_s}{\sigma_p} = \frac{3}{4}\left(\frac{p_d^{\mathrm{cm}}}{p_p^{\mathrm{cm}}}\right)^2, \quad (8)$$

where σ_s and σ_p are, respectively, the cross sections of the reactions Eqs. (4) and (7), and $p_p^{\mathrm{cm}}(p_d^{\mathrm{cm}})$ is the c.m. momentum of the proton (deuteron). All these quantities should be taken at the same c.m. total energy $\sqrt{s}$. The numerical coefficient in the right hand side of Eq. (8) is the ratio of spin degeneracy weights of particles in the final and initial states of the reaction Eq. (4).

Let us further apply the relations of relativistic kinematics

$$\begin{aligned} s &= 2m(^{13}\mathrm{C})E_p^{\mathrm{lab}} + [m_p + m(^{13}\mathrm{C})]^2 \\ &= 2m(^{12}\mathrm{C})E_d^{\mathrm{lab}} + [m_d + m(^{12}\mathrm{C})]^2, \end{aligned} \quad (9)$$

where E_i^{lab} is the kinetic energy of particles $i = p, d$ in the laboratory frame. The threshold proton energy for the reaction Eq. (4) is obtained from Eq. (9) by substituting $E_d^{\mathrm{lab}} = 0$. Then we obtain that $\sigma_s \neq 0$ at E_p^{lab} above 2.934 MeV, which is slightly larger than $|Q|$ value determined in Eq. (6). Analogous calculation for the reaction Eq. (5) shows that the latter has the threshold proton energy 14.568 MeV.

To calculate the ratio σ_s/σ_p one can use the kinematic relation

$$\frac{p_d^{\mathrm{cm}}}{p_p^{\mathrm{cm}}} = \frac{p_d^{\mathrm{lab}}}{p_p^{\mathrm{lab}}} \times \frac{m(^{12}\mathrm{C})}{m(^{13}\mathrm{C})} \simeq \sqrt{\frac{m_d E_d^{\mathrm{lab}}}{m_p E_p^{\mathrm{lab}}}}\,\frac{m(^{12}\mathrm{C})}{m(^{13}\mathrm{C})}. \quad (10)$$

Here the last equality is written in the nonrelativistic approximation. As an example, let us consider the deuteron production with energy $E_d^{\mathrm{lab}} = 1\,\mathrm{MeV}$ in the stripping reaction Eq. (4). According to Ref. [23] the inverse reaction Eq. (7) has the cross section $\sigma_p \simeq 6\,\mathrm{mb}$ at this bombarding energy. From Eq. (9) one can calculate the corresponding energy of protons in the reaction Eq. (4), which equals $E_p^{\mathrm{lab}} = 3.857\,\mathrm{MeV}$. Using further Eq. (10), one obtains the value $\sigma_s \simeq 0.330\,\sigma_p \simeq 2\,\mathrm{mb}$.

Note that many C-containing groups are present in the UDMA molecules. E.g., the methyl group CH_3 is frequent at the sides and ends of the UDMA molecule. The methyl group is bound to the rest of the molecule by a single covalent bond ($-CH_3$). In these groups the transition of a neutron from C to the H is especially easy, occurring via the reaction

$$\begin{aligned} {}^{13}\mathrm{CH_3} &\to ({}^{12}\mathrm{C}{+}n)(\mathrm{H_2}{+}p) \\ &\to {}^{12}\mathrm{CH_2}{+}(p{+}n) \to {}^{12}\mathrm{CH_2}{+}D. \end{aligned} \quad (11)$$

In vacuum this reaction is also endothermic, requiring 2.85 MeV additional energy. (If doubled it is $2 \times (CH_3 + H) \to C_2H_4 + 2D$, where C_2H_4 is ethylene). Similar transmutation is possible with the methylene group CH_2. This group is connected to the remainder of the molecule by two single bonds $-CH_2-$ (methylene bridge) or $CH_2=$. The same reaction with the methylene group is producing D and C_2H_2 (acetylene). Observing ethylene or acetylene as byproducts after the laser pulse irradiation, would confirm this mechanism of the intramolecular nucleon exchange.

C. Laser-induced proton acceleration

It is well known that energetic laser beams may strip electrons, which then pull protons from the target and accelerate them to multi-MeV energy [27–29]. In this section we argue that parameters of the NAPLIFE laser pulse may be sufficient to drive the $^{13}\mathrm{C}(p,d)^{12}\mathrm{C}$ reaction in the UDMA target and, therefore, to contribute to the observed formation of deuterium. Below we use simple electrostatic arguments to estimate the maximal kinetic energy of accelerated protons.

The important laser parameters are related by the formula for the laser intensity

$$I_L = 4E_L/\left(\pi d_L^2 \tau_L\right), \quad (12)$$

where E_L is the total beam energy, τ_L is the duration of the laser pulse, and d_L is the diameter of the focal spot.

For our estimates we use the following values (see Refs. [10,12])[4]: $I_L = 5 \times 10^{17}\,\mathrm{W/cm^2}$, $E_L = 25\,\mathrm{mJ}$, $d_L = 12.6\,\mu\mathrm{m}$, the laser wave length $\lambda_L = 0.795\,\mu\mathrm{m}$, and $\tau_L = 40\,\mathrm{fs}$.

With these laser parameters one can expect that only a small fraction of laser energy η goes to stripping of electrons from the target's atoms. The reason is that laser photons have relatively low energies, only of about 1.56 eV. Therefore, a single hydrogen atom can be ionized if its electrons absorb at least 9 photons.

It is assumed that free electrons are accelerated by the laser field via the ponderomotive force proportional to $\boldsymbol{j} \times \boldsymbol{B}$. Although this process is rapid and nonequilibrium, one can introduce an *effective specific energy* of an accelerated electron Θ. It is estimated by using the scaling relation suggested in Ref. [30], assuming thermalization of absorbed laser energy:

$$\Theta \simeq 0.42\, m_e c^2 \left(\frac{I_L \lambda_L^2}{I_0 \lambda_0^2}\right)^{1/3}, \quad (13)$$

where m_e is the electron mass, and $I_0 = 10^{18}\,\mathrm{W/cm^2}$, $\lambda_0 = 1\,\mu\mathrm{m}$. Substituting the parameters specified above, one gets $\Theta \simeq 146\,\mathrm{keV}$.

[3]Here we use numerical values of atomic masses from Ref. [22].

[4]Actually, the laser intensity has a certain (presumably, Gaussian) radial profile with a maximum $I_{\max}$ at the beam axis. We replace it by a rectangular profile with a hight of $0.5\,I_{\max}$.

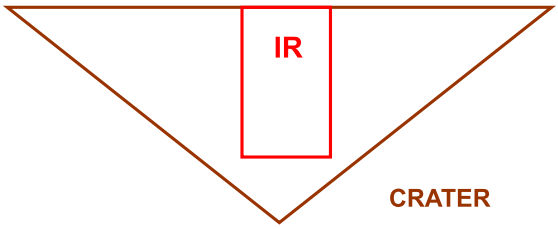

FIG. 4. Schematic cross section of the final crater (C) and the laser irradiation region (IR). The energy and momentum of the laser beam is initially absorbed in the IR.

We further assume that ionization electrons occupy initially the "irradiation region" (IR), which has approximately a cylindrical shape with the axis along the beam direction, as schematically shown in Fig. 4. Its diameter is approximately equal to the laser focal spot and its depth does not exceed the crater depth. The initial IR is smaller than the finally measured crater dimensions, since part of the absorbed laser energy is spent for heating and evaporating the surrounding matter.

Neglecting the three-dimensional (3D) expansion effects, one can estimate the length of IR as

$$L_{ir} \simeq c\tau_L = 12\,\mu\text{m}. \tag{14}$$

The radius of this cylinder is estimated as

$$R_{ir} \simeq \sqrt{\frac{E_L}{\pi I_L \tau_L}} \simeq 6.3\,\mu\text{m}, \tag{15}$$

which agrees with the observed diameter of the laser focus $d_L = 12.6\,\mu\text{m}$ [12]. The volume of the IR is

$$V_{ir} = \pi R_{ir}^2 L_{ir} \simeq 1496\,\mu\text{m}^3. \tag{16}$$

In this volume the original number of H atoms in UDMA is

$$N_{ir}^H = V_{ir} \times n_U \times 38 = 1.36 \times 10^{14}, \tag{17}$$

where $n_U = 1.5 \times 10^{21}\,\text{cm}^{-3}$ is the UDMA number density in the target.

By using the energy conservation, one can find the total number of stripped (ionization) electrons in the IR N_{ir}^e as

$$N_{ir}^e = \eta \frac{E_L}{\Theta}. \tag{18}$$

The parameter η is estimated by using the empirical formula of Ref. [28]:

$$\eta = 0.025\,(I_L/I_0)^{\,0.74}. \tag{19}$$

We assume that free electrons leave quickly the IR before protons and heavier ions start to accelerate. Then using the electroneutrality, one can estimate the net positive charge of this region as eN_{ir}^e where e is the proton charge. From Eqs. (18), (19), and (13), one obtains the total positive charge number of IR (in units of e) as

$$N_0 \simeq N_{ir}^e \simeq 1.60 \times 10^{10}. \tag{20}$$

This leads to the following estimate for the Coulomb potential acting on protons

$$U \sim \frac{eN_0}{R_{ir}}. \tag{21}$$

Under influence of the Coulomb field, protons (located initially inside the IR) acquire an additional energy of the order of eU. This leads to the maximal kinetic energy of protons

$$E_p \sim eU \simeq 3.65\,\text{MeV}. \tag{22}$$

By substituting the above energy into Eq. (9) one obtains that the maximal deuteron energy in the reaction Eq. (4) is about 1 MeV.

At later stages of the target evolution one can expect smaller values of acceleration due to expansion of the initially produced plasma. It will be demonstrated in the next section that the local charge density will significantly increase in the vicinity of NPs, if they are embedded in the target material. Then one can get larger proton energies as compared to that estimated in Eq. (22). Moreover, proton energies may even exceed the threshold values for the reaction Eq. (5).

IV. THE ROLE OF NANOROD ANTENNAS

The NAPLIFE experiments investigated the effect of golden NPs implanted in UDMA targets. At 25 mJ pulse energy in the case of Au1, about 7−9% deuterium abundance was detected [18] compared to the observed amount of hydrogen atoms in the emitted plum created after the laser shot.

The EPOCH PIC estimates [16,17] concluded that a single nanorod antenna with dimensions 85 nm × 25 nm increases the electromagnetic field intensity (in the NP's vicinity) by a factor of 25.9 (see Eq. (3) in Ref. [16]). Note however, that this result has been obtained for relatively low intensity $I_L = 4 \times 10^{15}\,\text{W/cm}^2$.

According to these calculations, initially about 10^3 electrons fluctuate between the ends of the resonant nano-antenna, with transverse peak momentum of about 0.15 MeV/c. The estimated maximal potential gradient is approximately 2.9 kV/nm.

Light absorption by embedded NPs was modeled earlier at 1000-fold larger laser energy in Ref. [31]. However, the obtained electric field (about 11.3 V/nm) is by more than two orders of magnitude less than in our estimate. The main reason is that nonresonant antenna/frequency combination was used! This indicates the importance of the use of resonant antennas. Such features are well known for classical antennas in radio communication.

Of course, the orientation of antennas with respect to the beam direction is rather important. Unfortunately, at present, the NAPLIFE target manufacturing does not produce oriented nano-antenna implantation.

Recently, the proton acceleration up to 93 MeV energy has been obtained with the PHELIX laser at GSI [27]. However, proton energies exceeding 20 MeV were achieved in these experiments only for $I_L > 10^{20}\,\text{W/cm}^2$. We expect that employing targets with properly oriented, resonant nano-antennas may produce 10–20 MeV protons even at lower intensities $I_L \lesssim 10^{17}\,\text{W/cm}^2$.

The increased energy and momentum absorption, as well as the enhanced pulse intensity may lead to a significant increase of the proton acceleration in the vicinity of a nanorod.

Under the influence of electromagnetic field, a single NP will be ionized, emitting some amount of electrons ΔN_s. Let

us express the number of ionization electrons as

$$\Delta N_s = \xi N_{\rm Au}, \tag{23}$$

where $N_{\rm Au}$ is the number of atoms in a single NP, and ξ is the ratio of the ionized electrons per golden atom.[5] According to calculations of Ref. [32], made for laser irradiated golden foils, one can expect the values $\xi \sim 30$ at laser intensities $I_L \gtrsim 10^{18}$ W/cm^2. We consider ξ as a parameter, although it may depend on characteristics of the laser, orientation and sizes of NPs, etc.

A proton located near the surface of a charged nanorod gets an additional Coulomb energy

$$\Delta E \sim \frac{2e^2\,\Delta N_s}{l_{\rm min}} \sim 290\,\xi\,{\rm keV}, \tag{24}$$

where $l_{\rm min} = 25$ nm is the diameter of the nanorod. In the numerical estimate we have taken $N_{\rm Au} \simeq 2.46 \times 10^6$.

We can also estimate the Coulomb energy per atom of the ionized NP as

$$\frac{E_C}{N_{\rm Au}} \sim \frac{2\,(e\Delta N_s)^2}{N_{\rm Au} l_{\rm min}} \simeq 290\,\xi^2 {\rm keV}. \tag{25}$$

If ξ is not too small, this energy will exceed the typical "binding" energy ~10 eV per atom in a nonexcited NP. According to Eq. (25), this occurs at $\xi \gtrsim 6 \times 10^{-3}$. In this case such NPs will be destroyed due to Coulomb-induced explosion.

It is interesting to estimate the additional (positive) charge provided by nanoparticles in the IR. It is equal to $e\,\Delta N_s N_{ir}^{(NP)}$ where

$$N_{ir}^{(NP)} \simeq \frac{V_{ir}}{\langle L_{\rm Au2}\rangle^3} \simeq 3850 \tag{26}$$

is the number of NPs in the IR. In the second equality we substituted the volume of the IR V_{ir} from Eq. (16) and the average distance between nanorods $\langle L_{\rm Au2}\rangle$ obtained in Sec. II B. Again we give numerical estimates for the case Au2.

Due to appearance of the additional charge, protons get larger acceleration in targets with NPs. Instead of Eqs. (21) and (22) we obtain the following estimate for the proton energy

$$E_p \sim \frac{e^2(N_0 + \Delta N)}{R_{ir}} \simeq (3.65 + 2.15\,\xi)\ {\rm MeV}, \tag{27}$$

where

$$\Delta N = \Delta N_s N_{ir}^{(NP)} \simeq 9.5 \times 10^9\,\xi \tag{28}$$

is the additional charge (in units of e) of the IR due to the presence of ionized nanorods.

At large enough ξ many deuteron-production processes with threshold energies larger than for the reaction Eq. (4) may be open. For example, at $\xi \sim 10$ one gets almost sevenfold increase of proton energy, i.e., $E_p \simeq 22$ MeV, which is above the threshold energy of the reaction Eq. (5). As compared to the case without NPs, where the number of ionized protons $N_p \simeq N_0 \lesssim 10^{-4} N_{ir}^H$ is relatively small, at $\xi \gtrsim 10$ one can expect much larger N_p–values for targets with nanorods.

[5] At $\xi \lesssim 1$ ionization electrons come mainly from the conductivity zone of the Au metal.

Recently [33], we have performed kinetic simulations of the dynamics of nanorod electrons under the influence of the laser beam. For this purpose we have used the EPOC code to study spectra of free protons accelerated by a single NP embedded in a plastic target. Two values of a laser pulse intensity, $I_L = 4 \times 10^{15}$ and $I_L = 4 \times 10^{17}$ W/cm^2, have been considered. In both cases we obtain maximal proton energies in the range 1–10 MeV. This agrees with above estimates for $\xi \sim 10$.

V. ESTIMATION OF DEUTERON TO PROTON RATIO

A. Rate equations for deuteron production

As discussed above, initially, ionization electrons and protons are produced in the cylindrical channel, which is much more narrow than the crater. We approximate the latter as a cone with radius R_C and the depth L_C (see Fig. 4). According to NAPLIFE data the volume of the crater for case Au2 can be estimated as

$$V_C = \tfrac{1}{3}\pi R_C^2 L_C \simeq 452\,400\ \mu{\rm m}^3, \tag{29}$$

where we have substituted the values $R_C = 120\,\mu$m and $L_C = 30\,\mu$m. One can see that V_C is about 300 times larger than the volume of the cylindrical irradiation channel [Eq. (16)].

The ionized protons are produced in the cylindrical channel in a short time interval $t \lesssim \tau_L \sim 40$ fs. At later times these protons propagate through the UDMA material and may induce transmutation reactions in the whole crater volume. Propagation of the produced protons with the energy $E_p = m_p v^2/2 = 4$ MeV through the crater volume takes time

$$t_C \simeq \frac{R_C}{v} = \frac{120\,\mu{\rm m}}{0.092\,{\rm c}} \simeq 4.35\ {\rm ps}, \tag{30}$$

where m_p and v are, respectively, the mass and velocity of the proton.

The number of deuterons, which can be produced by the stripping reaction Eq. (4) can be estimated by using a simple rate equation

$$\frac{dN_d}{dt} = \langle\sigma_s v\rangle\, n_{13\rm C} \times n_p(t) V(t), \tag{31}$$

where σ_s is the cross section of the reaction Eq. (4), $n_{13\rm C} \simeq$ const is the number density of ^{13}C in the UDMA matter, and $V(t)$ is the volume occupied by the ionization protons.

Obviously, after a short initial stage $t > \tau_L$ the total number of protons remains the same, but their density drops, such that $N_p = n_p V(t) = {\rm const}$, where N_p is given by Eq. (20). Therefore, all terms in the right hand side of Eq. (31) are approximately time independent and one may write its solution at $t > \tau_L$ as

$$\frac{N_d(t)}{N_p} = \langle\sigma_s v\rangle\, n_{13\rm C} \times (t - \tau_L) \tag{32}$$

Now we can estimate the d/p ratio taking $t - \tau_L \sim t_C$, choosing the input parameters: $\sigma_s \simeq 2$ mb, $v \simeq 0.092\,c \simeq 2.76 \times 10^9$ cm/s (at $E_p \simeq 4$ MeV), and substituting $n_{13\rm C} = 3.66 \times 10^{20}$ cm^{-3}. Finally we get the following ratio (for the case Au2)

$$\frac{N_d}{N_p} = 5.52 \times 10^{-18}\frac{\rm cm^3}{\rm s} \times 3.66 \times 10^{20}\frac{1}{\rm cm^3} \times 4.35 \times 10^{-12}{\rm s} \simeq 8.8 \times 10^{-9}. \tag{33}$$

Now let us estimate the d/p radio for the reaction Eq. (5). One can do this using the Eqs. (31) and (32), but replacing n_{13C} by the two-order of magnitude larger density of ^{12}C nuclei $n_{12C} \simeq 3.41 \times 10^{22}\,\mathrm{cm}^{-3}$, and substituting the cross section σ_s of the reaction Eq. (5). For a rough estimate we choose the proton energy $E_p = 20\,\mathrm{MeV}$ and the cross section $\sigma_s \simeq 25\,\mathrm{mb}$ from Ref. [34]. Then, instead of Eq. (33) one obtains the estimate

$$\frac{N_d}{N_p} = 1.55 \times 10^{-16}\frac{\mathrm{cm}^3}{\mathrm{s}} \times 3.41 \times 10^{22}\frac{1}{\mathrm{cm}^3} \times 1.94 \times 10^{-12}\mathrm{s} \simeq 1.02 \times 10^{-5}, \tag{34}$$

which is by a factor 1160 larger than the d/p ratio for the reaction Eq. (4).

Nevertheless, both d/p values are too small to explain the D/H ratios extracted from the LIBS spectra [10,18]. Note that both ratios are below the background ratio $\frac{N_D}{N_H} = 1.6 \times 10^{-4}$ in the Earth atmosphere under normal conditions.

However, one should bear in mind that to be visible in LIBS spectra, protons and deuterons should form neutral H and D atoms by recombination with electrons in the UDMA target. Therefore, the LIBS measurements give only indirect information about the abundances of ionized deuterons and protons, produced by the irradiation of UDMA targets. It is clear that the recombination process will shift the D/H ratio to larger values. The reason is that deuterons produced in reactions Eqs. (4), (5) have significantly lower velocities as compared to protons. But, the recombination cross section increases with decreasing particle velocity. Therefore, the recombination probability for deuterons will be larger than for protons.

B. Role of electron-ion recombination

To estimate the numbers of the atomic hydrogen (H) and deuterium (D) one can use the rate equations similar to Eq. (31), but replacing σ_s by the recombination cross section σ_r and n_{13C} by the electron density n_e. Then the ratio D/H will be given by the equation similar to Eq. (32) with the replacements $n_{13C} \to n_e$ and $\sigma_s \to \sigma_r$.

To get the quantitative estimate, we assume that recombination lengths for protons and deuterons are longer than the crater size $\sim$100 μm. Then the ratio of recombination probabilities will be approximately equal to the ratio of recombination cross sections. According to Ref. [35], they are inversely proportional to the fifth power of the ion velocity [36]. Finally, we obtain the approximate relation

$$\frac{\mathrm{D}}{\mathrm{H}} \sim \left(\frac{m_d E_p}{m_p E_d}\right)^{5/2}\frac{d}{p}. \tag{35}$$

Note that we have assumed that propagation times of proton and deuterons in the target are inversely proportional to ion velocities. Now we can calculate the D/H ratios for two stripping reactions Eqs. (4) and (5) considered before.

For the reaction Eq. (4), taking $E_p = 4\,\mathrm{MeV}$ and $E_d = 1\,\mathrm{MeV}$, one has from Eqs. (33) and (35)

$$\frac{\mathrm{D}}{\mathrm{H}} \sim 181 \times \frac{d}{p} \simeq 1.6 \times 10^{-6}. \tag{36}$$

One can see that this reaction still gives too small D/H ratio even if one takes into account the recombination corrections.

In the case of the reaction Eq. (5), substituting $E_p = 20\,\mathrm{MeV}$, $E_d = 5.92\,\mathrm{MeV}$ [this value follows from Eq. (9)], and using Eqs. (34) and (35), one gets the estimate

$$\frac{\mathrm{D}}{\mathrm{H}} \sim 118 \times \frac{d}{p} \simeq 1.2 \times 10^{-3}. \tag{37}$$

This value is still below experimental ratios for the Au2 target, but it is much closer to them. We believe that better agreement with observed data can be achieved by fine tuning of model parameters, in particular, the ionization fraction of Au atoms. Also, we are going to take into account feeding of the Balmer-α states from higher atomic levels.

As mentioned above, both H and D yields observed in NAPLIFE experiments show strong event-by-event fluctuations. There are several possible reasons for such fluctuations. First, the total number of NPs in the IR is rather small: $N_{ir}^{(NP)} \lesssim 4000$ [see Eq. (26)] for Au2 target. In accordance with the Poisson statistics one can expect relative fluctuations of ionized proton spectra on the level of several percent. Second, even stronger fluctuations may be caused by random orientations of nanorods with respect to the laser beam. In particular, this will cause fluctuations of the gold ionization parameter ξ introduced in Eq. (23). Finally, recombination rates of accelerated protons and deuterons may also exhibit even-by-event fluctuations. We plan to study these effects in the future.

VI. CONCLUSION AND OUTLOOK

In the present article we have analyzed the results of NAPLIFE experiments on laser irradiation of polymer targets. They show a significant formation of deuteron atoms at high enough laser pulse energies. The deuteron's yield increases with the concentration of implanted nanoparticles.

In our analysis we have focused on the possibility of nuclear transmutation mechanisms, namely due to the stripping reactions $p + \mathrm{C} \to d + X$ with the carbon isotopes ^{12}C and ^{13}C. It is argued that proton energies achievable in the laser-target interaction are sufficient for deuteron formation in such reactions, especially for targets with implanted golden NPs.

Our model does not take into account that spatial distributions of D and H atoms in Balmer states may change differently due to scatterings in target plasma. Therefore, the above comparison with LIBS measurements should be regarded with caution. In the future we plan to perform more realistic kinetic calculations including scattering effects.

Additional investigations are necessary for verifying our results. First, it would be desirable to reproduce our observations at higher laser energies, e.g., at GSI/FAIR PHELIX and future ELI-ALPS facilities. Additional diagnostics tools would be desirable, including measurements of x rays, neutrons, α particles, etc. We plan to perform new experiments with different pulse widths, target thickness, and profiles of NPs.

On the theoretical side, the numerical modeling of target plasma evolution is necessary to estimate yields of secondary particles and their momentum distributions. Special investigation should be made to study properties of hot spots

created by nanoparticles, and their role in the nuclear transmutation.

Finally, we would like to note that with some modifications the considered setup can be also used for enhancing fusion reactions. A solid D+T target with embedded Au nanoparticles can be irradiated by two laser beams from opposite sides, as first proposed in Ref. [4]. As demonstrated above, the implanted nanoparticles generate electrostatic potentials, which can accelerate d and t ions to kinetic energies of about 10 MeV. This is sufficient to ignite fusion reactions, e.g., $d + t \rightarrow He + n$, with the energy gain of 17.6 MeV.

ACKNOWLEDGMENTS

Enlightening discussions with Miklós Kedves, Márk Aladi, and Oliver A. Fekete are gratefully acknowledged. L.P.C. acknowledges support from Wigner Research Center for Physics, Budapest (Grant No. 2022-2.2.1-NL-2022-00002). T.S.B., M.C., N.K., I.P., A.S., and D.V. acknowledge support by the National Research, Development and Innovation Office of Hungary. H.S. acknowledges the Judah M. Eisenberg Professor Laureatus chair at Fachbereich Physik of Goethe Universität Frankfurt. We would like to thank the Wigner GPU Laboratory at the Wigner Research Center for Physics for providing support in computational resources. This work is supported in part by the Frankfurt Institute for Advanced Studies, Germany, the Eötvös, Loránd Research Network of Hungary, the Research Council of Norway, Grant No. 255253, and the National Research, Development and Innovation Office of Hungary, for projects: Optimized nanoplasmonics (Project No. K116362), and Ultrafast physical processes in atoms, molecules, nanostructures and biological systems (Project No. EFOP-3.6.2-16-2017-00005).

[1] L. P. Csernai, Detonation on timelike front for relativistic systems, Zh. Eksp. Teor. Fiz. **92**, 397 (1987) [Sov. Phys. JETP **65**, 219 (1987)].

[2] L. P. Csernai and D. D. Strottman, Volume ignition via time-tike detonation in pellet fusion, Laser Part. Beams **33**, 279 (2015).

[3] L. P. Csernai, N. Kroó, and I. Papp, Procedure to improve the stability and efficiency of laser-fusion by nano-plasmonics method. Patent Note # P1700278/3 at the Hungarian Intellectual Property Office (2017).

[4] L. P. Csernai, M. Csete, I. N. Mishustin, A. Motornenko, I. Papp, L. M. Satarov, H. Stöcker, and N. Kroó (NAPLIFE Collaboration), Radiation dominated implosion with flat target, Phys. Wave Phen. **28**, 187 (2020).

[5] L. P. Csernai, N. Kroó, and I. Papp, Radiation-dominated implosion with nano-plasmonics, Laser Part. Beams **36**, 171 (2018).

[6] J. Zhang, W. M. Wang, X. H. Yang, D. Wu, Y. Y. Ma, J. L. Jiao, Z. Zhang, F. Y. Wu, X. H. Yuan, Y. T. Li, and J. Q. Zhu, Double-cone ignition scheme for inertial confinement fusion, Philos. Trans. R. Soc. A **378**, 20200015 (2020).

[7] G. Zhang, M. Huang, A. Bonasera, Y. G. Ma, B. F. Shen *et al.*, Nuclear probes of an out-of-equilibrium plasma at the highest compression, Phys. Lett. A **383**, 2285 (2019).

[8] M. Csete, A. Szenes, E. Tóth, D. Vass, O. Fekete, B. Bánhelyi, I. Papp, T. Bíró, L. P. Csernai, N. Kroó (NAPLIFE Collaboration), Comparative study on the uniform energy deposition achievable via optimized plasmonic nanoresonator distributions, Plasmonics **17**, 775 (2022).

[9] N. Kroó, for NAPLIFE Collaboration, High field nanoplasmonics, invited talk at the Margaret Island Symposium 2022 on Vacuum Structure, Particles, and Plasmas, Budapest, May 15–18, 2022.

[10] P. Rácz, for NAPLIFE Collaboration, LIBS spectra from polymer shootings, invited talk at the Margaret Island Symposium 2022 on Vacuum Structure, Particles, and Plasmas, Budapest, May 15–18, 2022.

[11] http://pubchem.ncbi.nlm.nih.gov/compound/170472.

[12] Á. Nagyné Szokol, for NAPLIFE Collaboration, Effect of the embedded plasmonic gold nanorods on the interaction of high intensity laser irradiation with UDMA polymer - the volume loss during crater formation, talk at 11th International Conference on New Frontiers in Physics 2022, Kolymbari, Crete, Greece, 30 August–11 September 2022.

[13] J. Kámán *et al.*, for NAPLIFE Collaboration, Gold nanorods induced nanoplasmonic effect on structural changes during high intensity laser irradiation of UDMA polymer, talk at 10th International Conference on New Frontiers in Physics 2021, Kolymbari, Crete, Greece, 23 August–7 September 2021.

[14] M. Veres, for NAPLIFE Collaboration, Raman spectroscopy of laser-matter interactions, invited talk at the Margaret Island Symposium 2022 on Vacuum Structure, Particles, and Plasmas, Budapest, May 15–18, 2022.

[15] M. Kedves and M. Aladi (private communication).

[16] I. Papp, L. Bravina, M. Csete, A. Kumari, I. N. Mishustin, D. Molnár, A. Motornenko, P. Rácz, L. M. Satarov, H. Stöcker, D. D. Strottman, A. Szenes, D. Vass, T. S. Biró, L. P. Csernai, and N. Kroó (NAPLIFE Collaboration), Kinetic model evaluation of the resilience of plasmonic nanoantennas for laser-induced fusion, PRX Energy **1**, 023001 (2022).

[17] I. Papp, L. Bravina, M. Csete, A. Kumari, I. N. Mishustin, A. Motornenko, P. Rácz, L. M. Satarov, H. Stöcker, D. D. Strottman, A. Szenes, D. Vass, A. N Szokol, J. Kámán, A. Bonyár, T. S. Biró, L. P. Csernai, and N. Kroó (NAPLIFE Collaboration), Kinetic model of resonant nanoantennas for laser induced fusion, Front. Phys. **11**, 1116023 (2023).

[18] A. Kumari, for NAPLIFE Collaboration, LIBS analysis of the polymer UDMA, talk at 11th International Conference on New Frontiers in Physics 2022, Kolymbari, Crete, Greece, 30 August–11 September 2022.

[19] These results are rather preliminary. The detailed analysis of LIBS spectra will be published in a separate paper.

[20] Note, that $p \rightarrow n$ conversion may also occur by capturing electrons from bound atomic states. However, such processes are slow and may occur only for sufficiently heavy atoms.

[21] One can also consider the deuteron production in exothermic reactions $p + p \rightarrow d + e^+ + \bar{\nu}_e$. But this weak reaction has nonzero Coulomb barrier and the corresponding cross section is relatively small.

[22] M. Wang, W. J. Huang, F. G. Kondev, and S. Naimi, The AME2020 atomic mass evaluation (II). Tables, graphs and references, Chin. Phys. C **45**, 030003 (2021).

[23] G. C. Phillips, The long-range protons from the disintegration of carbon by deuterons and a study of the competing reactions, Phys. Rev. **80**, 164 (1950).

[24] E. Kashy, R. R. Perry, and J. R. Risser, Excited states in N^{14} from $C^{12}(d,d)C^{12}$, $C^{12}(d,p_0)C^{13}$ and $C^{12}(d,p_1)C^{13*}$, Phys. Rev. **117**, 1289 (1960).

[25] P. E. Hodgson and D. Wilmore, Reactions from 1 to 5 MeV deuterons on carbon, Proc. Phys. Soc. **90**, 361 (1967).

[26] L. D. Landau and E. M. Lifshitz, *Quantum Mechanics. Non-relativistic Theory* (Pergamon, Oxford, 1977).

[27] J. Hornung, Y. Zobus, P. Boller, C. Brabetz, U. Eisenbarth, T. Kühl, Zs. Major, J. B. Ohland, M. Zepf, B. Zielbauer, and V. Bagnoud, Enhancement of the laser-driven proton source at PHELIX, High Power Laser Sci. Engineering **8**, e24 (2020).

[28] M. Roth and M. Schollmeier, Ion acceleration − target normal sheath acceleration, arXiv:1705.10569.

[29] I. Papp, L. Bravina, M. Csete, I. N. Mishustin, D. Molnár, A. Motornenko, L. M. Satarov, H. Stöcker, D. D. Strottman, A. Szenes, D. Vass, T. S. Biro, L. P. Csernai, N. Kroó (NAPLIFE Collaboration), Laser Wake Field Collider, Phys. Lett. A **396**, 127245 (2021).

[30] A. Poyé, S. Hulin, J. Ribolzi, M. Bailly-Grandvaux, F. Lubrano-Lavaderci, M. Bardon, D. Raffestin, J. J. Santos, and V. Tikhonchuk, Thin target charging in short laser pulse interactions, Phys. Rev. E **98**, 033201 (2018).

[31] A. Plech, V. Kotaidis, M. Lorenc, and J. Boneberg, Femtosecond laser near field ablation from gold nanoparticles, Nat. Phys. **2**, 44 (2006).

[32] D. Kawahito and Y. Kishimoto, Ionization and acceleration of multiply charged gold ions in solid film irradiated by high intensity laser, Phys. Plasmas **27**, 033108 (2020).

[33] I. Papp, for NAPLIFE Collaboration, Dynamical properties of nanorods embedded in fusion fuel with plasma simulation approach, invited talk at the Margaret Island Symposium 2023 on Vacuum Structure, Particles and Plasmas, Budapest, June 6–9, 2023.

[34] A. B. Whitehead and J. S. Foster, Activation cross sections for $C^{12}(p,pn)C^{11}$, $O^{16}(p,\alpha)N^{13}$, and $F^{19}(p,pn)F^{18}$, Can. J. Phys. **36**, 1276 (1958).

[35] I. A. Kotelnikov and A. I. Milstein, Electron radiative recombination with a hydrogen-like ion, Phys. Scr. **94**, 055403 (2019).

[36] For a rough estimate we assume that in recombination the target's electrons have much smaller velocities than ions.